

On the Effects of Ice Crystal Porosity on the Radiative Characteristics of Cirrus Clouds

GRAEME L. STEPHENS

Department of Atmospheric Science, Colorado State University, Fort Collins

This paper attempts to illustrate how the porous nature of ice crystals might influence the relationships between the radiative properties of ice clouds and the ice water path. Solutions of the electromagnetic wave equation were obtained for a simplified, hollow, infinitely long circular cylinder. On the basis of these solutions it was implied that the effects of ice crystal porosity on the particle-scattering parameters can be expected to be small and that the major influence of porosity on radiation-ice water path (IWP) relationships will be primarily on the definition of IWP. It is suggested that this effect probably accounts for the existing discrepancy noted in this paper between the theoretical and observed ϵ -IWP relationships.

1. INTRODUCTION

The problem of understanding the impact of cirrus clouds on the radiative budget of the atmosphere is complicated by the complex microphysical characteristics of such clouds. Such clouds are composed of nonspherical ice crystals [e.g., *Heymsfield, 1977*] in presumed low concentrations [*Heymsfield and Platt, 1984*] and often with some characteristic orientation [e.g., *Platt et al., 1978*]. The importance of the complicated transfer of radiation through these clouds is well illustrated in the modeling efforts of *Starr and Cox [1985]* and the general circulation model results of *Ramanathan et al. [1983]*, which suggest some influence not only on the evolution of the clouds themselves but also on certain aspects of the larger-scale atmospheric circulation. It is therefore important to establish in some way the effect of the above-stated complex microphysical aspects on the radiative transfer through these clouds, thus testing the utility of the existing and necessarily simple description of radiative transfer in atmospheric circulation models.

A typical example of such a simple parameterization for the infrared properties of both water and ice clouds is shown in Figure 1. The schemes illustrated relate the cloud emissivity to the cloud liquid or ice water path (IWP) in the manner shown. The collection of curves representing water clouds in Figure 1 is based in part on theory and in part on observation. The curves shown for cirrus clouds are derived from observations, with the exception of that of *Liou and Wittman [1979]*. As already noted by the authors of these studies, certain as yet unexplained discrepancies exist between the ice and water cloud relationships. There are still insufficient measurements to suggest whether or not similar discrepancies exist in the IWP albedo relationships.

The purpose of this paper is to consider yet another of the complexities of the microphysical characteristics of ice crystal clouds which has not been considered in the literature in the context of radiative transfer and which offers a plausible explanation for the existence of the discrepancies portrayed in Figure 1. It is well known [e.g., *Pruppacher and Klett, 1980*] that most ice crystals have bulk densities less than those of solid ice as a result of the existence of air bubbles within the

crystal. Columnar ice crystals, for example, are often hollow. An appreciation of the magnitude of this effect on the density of the ice crystal can be assessed by reference to Figure 2, taken from the work of *Heymsfield [1972]*. In Figure 2, the bulk density of individual ice crystals is shown as a function of maximum crystal dimension. Clearly, the density of the ice crystal differs substantially from that of solid ice; the difference being greatest for the largest ice particles.

The issue addressed in this paper concerns the likely effect of particle porosity on the scattering characteristics and, ultimately, the bulk radiative properties of a cloud composed of this type of crystal. The work reported here attempts to assess whether the discrepancies noted in Figure 1 result from the potential effect of crystal porosity on the scattering properties of the crystal, or from the incorrect inference of IWP, or both. To gain some overall assessment of this issue, a simple model of a hollow ice cylinder is considered and the solutions of Maxwell's equations are sought. This highly idealized model is meant only to test the hypothesis that crystal porosity is relevant to the relationships between bulk radiative transfer properties of the cloud and the IWP, as portrayed in Figure 1. The prevalence of columnar and bullet-shaped ice crystals with hollowed cores is well documented for cirrostratus clouds [e.g., *Heymsfield and Knollenberg, 1972*] and is to be expected from the temperature and humidity conditions typical of these clouds [e.g., *Pruppacher and Klett, 1982*]. The hypothetical ice crystal model chosen for this study is thus more realistic than either a solid columnar model or spherical ice crystal models.

In the following section the idealized model of a porous ice crystal is described and the solution of the electromagnetic wave equations is outlined. Results obtained from this theory for the extinction, scattering and absorption efficiencies, and the scattering phase functions for a few selected wavelengths are then presented.

2. SCATTERING OF ELECTROMAGNETIC RADIATION BY A HOLLOW ICE CRYSTAL

Consider the ice crystal as a hollow, infinitely long circular cylinder, as shown in Figure 3. The solution of Maxwell's equations for coaxial, infinitely long cylinders has many diverse applications and has been described, for example, by *Kerker and Matijevic [1961]* among others, for waves normally incident on the long axis of the cylinder. The problem of oblique incidence was addressed by *Samaddar [1970]*, who demonstrated that the problem has no general solution. In

Copyright 1987 by the American Geophysical Union.

Paper number 6D0666.
0148-0227/87/006D-0666\$05.00

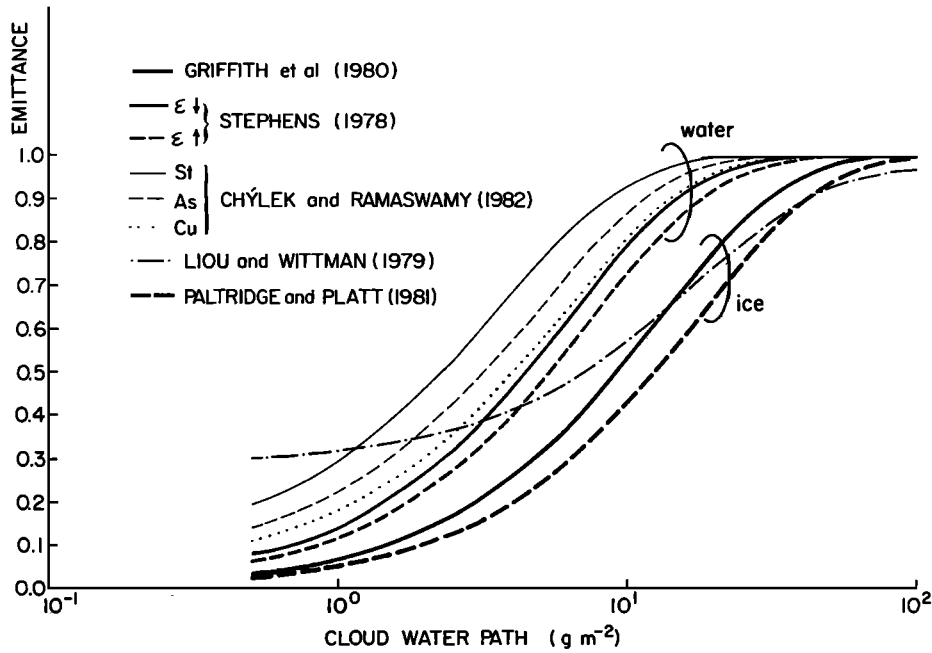


Fig. 1. The effective emissivity of a cloud layer as a function of liquid water path, as obtained from the cited studies. Distinction is made between ice and water clouds.

this present sensitivity study only the derived solutions for normally incident radiation are considered, but it is argued that the general nature of the results will be the same for all other incident directions.

In deriving the solution it is necessary to consider the radius of the core *a*, the radius of the shell *b*, and the refractive indices of the core *m*₂, shell *m*₁, and environment *m*₀, as shown in Figure 3. Also shown in Figure 3 are the two plane-polarized components of the incident beam and, by suitable linear superposition of the solutions for each of these cases, the solution for any arbitrary elliptically polarized incident wave can be determined. If we consider these two cases separately and define *u* and *v* as the solutions to the associated

scalar-wave equations to Case 1 and 2, respectively, then the following solutions apply.

Case 1. *E* Parallel to the Cylinder Axis
Axis

$$u = \sum_{n=-\infty}^{\infty} F_n [J_n(m_0 kr) - b_n^0 H_n(m_0 kr)] \quad r > b \quad (1)$$

$$u = \sum_{n=-\infty}^{\infty} F_n [B_n^1 J_n(m_1 kr) - b_n^1 H_n(m_1 kr)] \quad b > r > a \quad (2)$$

$$u = \sum_{n=-\infty}^{\infty} F_n [B_n^2 J_n(m_2 kr)] \quad r > a \quad (3)$$

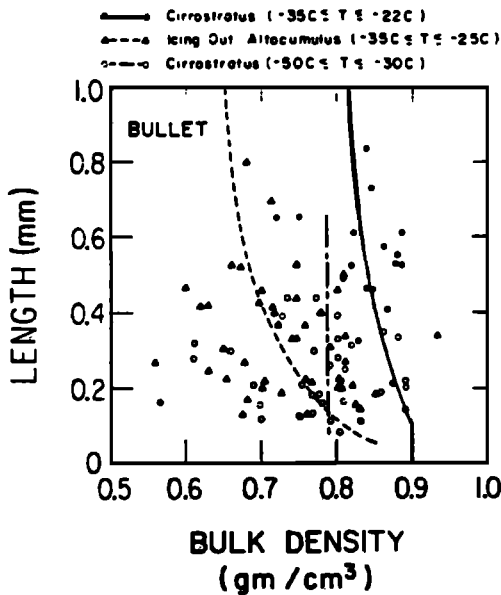


Fig. 2. The relationship between the bulk density of ice crystal dimension [from Heymsfield, 1972] without change.

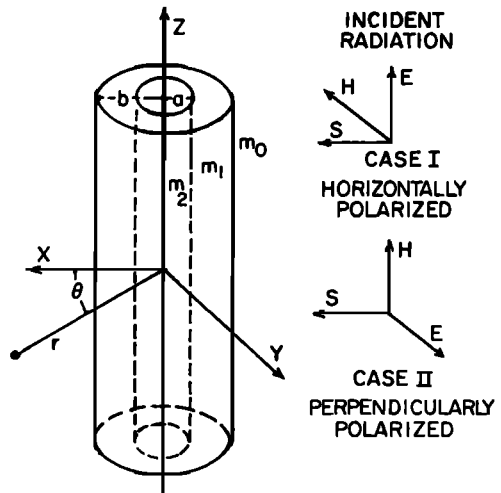


Fig. 3. Coordinates and vectors for scattering by a concentric cylinder. Here *a* and *b* are radii of the inner and outer cylinders, respectively, and *m*₀, *m*₁, and *m*₂ are the refractive indexes of the regions specified. *S*, *E*, and *H* are Poynting, electric, and magnetic vectors, respectively. Note that *θ* is the scattering angle.

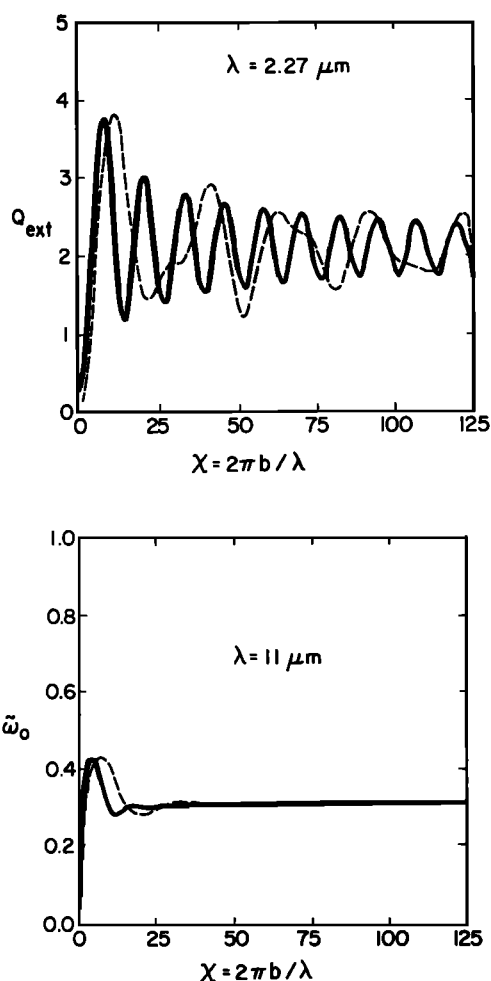


Fig. 4a. The extinction efficiency per unit length for a hollowed concentric ice cylinder (dashed curve) core with a 30% volume reduction and the extinction of a solid-core cylinder (solid curves). Both are shown as a function of the outer shell size parameter (kb) for the wavelengths indicated: (top) $\lambda = 2.27 \mu\text{m}$; (bottom) $\lambda = 11.0 \mu\text{m}$.

Case 2. H Parallel to the Cylinder Axis

$$v = \sum_{n=-\infty}^{\infty} F_n [J_n(m_0 kr) - a_n^0 H_n(m_0 kr)] \quad r > b \quad (4)$$

$$v = \sum_{n=-\infty}^{\infty} F_n [A_n^1 J_n(m_1 kr) - a_n^1 H_n(m_1 kr)] \quad b > r > a \quad (5)$$

$$v = \sum_{n=-\infty}^{\infty} F_n [A_n^2 J_n(m_2 kr)] \quad r > a \quad (6)$$

where $J_n(z)$ is the Bessel function of the first kind, $H_n(z)$ is the Hankel function of the second kind and F_n is the wave propagation factor

$$F_n = (-1)^n \exp(in\theta + i\omega t) \quad (7)$$

where $\omega/2\pi$ is the frequency, t is time, $k/2\pi$ is the wave number $1/\lambda$, θ is the scattering angle (refer to Figure 3) and a_n^0 , b_n^0 , $A_n^1 \dots$ are the eight undetermined coefficients.

In principle, this paper is only concerned with the field outside the particle which is due to the superposition of incident and scattered waves. Thus only Hankel functions are considered as solutions because of the necessary regularity at infinity. For the field in the inner or core region of the cylin-

der, only the Bessel function of the first kind is utilized because of its properties at the origin, while the field within the shell can be described by a combination of these two functions.

The undetermined coefficients and thus the complete solutions for u and v are obtained by observing the continuity of mu , $m\partial u/\partial r$, m^2v , and $\partial v/\partial r$ at the boundaries $r = a$ and $r = b$. Applying these conditions to (1)–(6), a set of eight equations is obtained from which the eight unknown coefficients are obtained in turn (see, for example, Kerker and Matijevic [1961] for details).

While it is straightforward to reduce the equations derived from the stated boundary conditions to obtain these coefficients, the expressions so derived are not generally in a form suitable for numerical computations. To overcome this, it is customary to introduce the logarithmic derivatives of the associated Bessel functions, which are introduced here as

$$\Psi_n(\beta) = \frac{J_n'(\beta)}{J_n(\beta)} \quad (8)$$

$$X_n(\beta) = \frac{H_n'(\beta)}{H_n(\beta)} \quad (9)$$

where the prime refers to differentiation of the function with respect to the argument. Since one is only interested in the

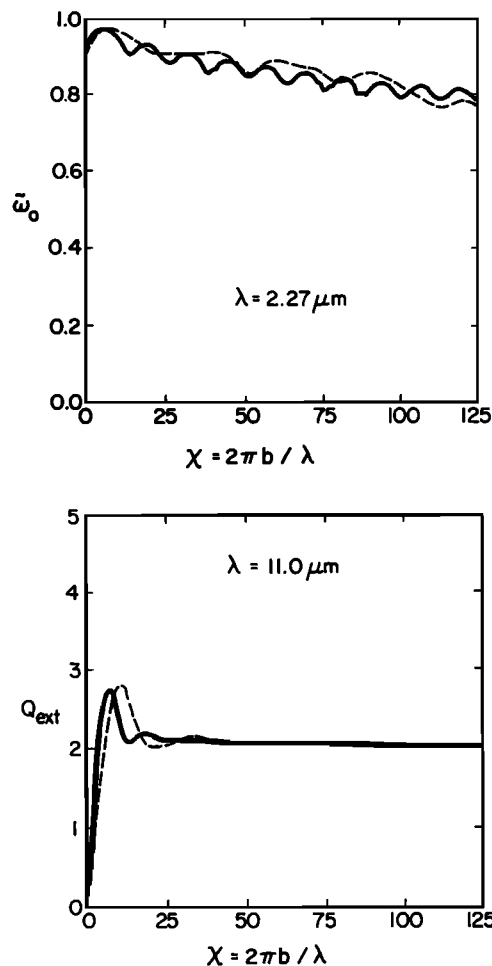


Fig. 4b. The single-scatter albedo as a function of the outer shell size parameter. The curves and wavelengths apply as for Figure 4a: (top) $\lambda = 2.27 \mu\text{m}$; (bottom) $\lambda = 11.0 \mu\text{m}$.

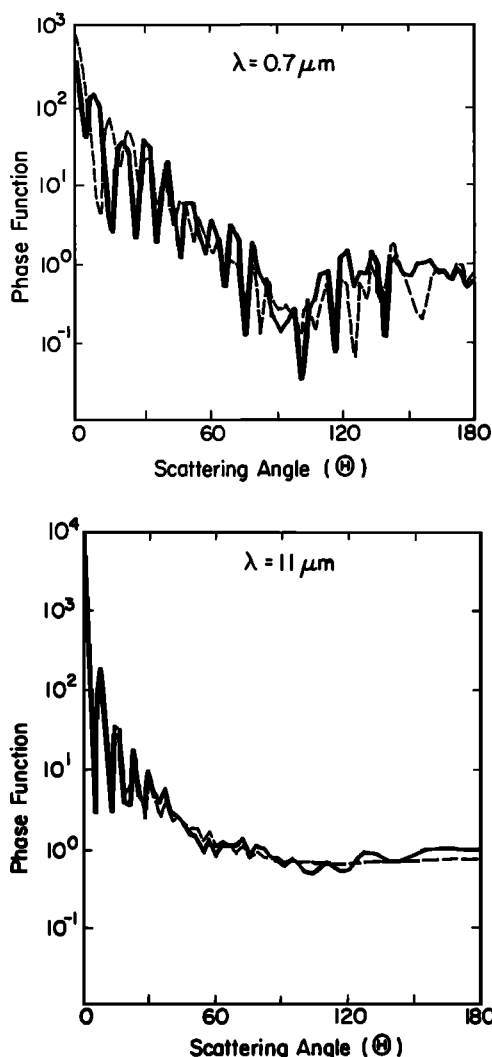


Fig. 5. The scattering phase function of a single concentric ice cylinder illuminated normal to its long axis as a function of scattering angle. The solid curve applies to a solid ice cylinder and the dashed curve to a hollow ice cylinder, where the radius of the hollow core is determined from the specified 30% reduction in the volume of the solid particle: (top) $\lambda = 0.7 \mu\text{m}$; (bottom) $\lambda = 11.0 \mu\text{m}$.

field for $r \gg b$, only the two coefficients a_n^0 and b_n^0 need be considered. These coefficients are expressed here in terms of the logarithmic derivatives (8) and (9) as

$$b_n^0 = \frac{J_n(\beta_0) [U_3 U_2 J_n(\beta_2) H_n(\beta_1) - U_4 U_1 H_n(\beta_2) J_n(\beta_1)]}{H_n(\beta_0) [U_2 U_5 J_n(\beta_2) H_n(\beta_1) - U_6 U_1 H_n(\beta_2) J_n(\beta_1)]} \quad (10)$$

and

$$a_n^0 = \frac{J_n(\beta_0) [U_9 U_7 H_n(\beta_1) J_n(\beta_2) - U_{10} U_8 J_n(\beta_1) H_n(\beta_2)]}{H_n(\beta_0) [U_{11} U_9 H_n(\beta_1) J_n(\beta_2) - U_{12} U_{10} J_n(\beta_1) H_n(\beta_2)]} \quad (11)$$

where

$$\begin{aligned} U_1 &= m_1 X_n(\beta_2) - m_2 \Psi_n(\beta_3) \\ U_2 &= m_1 \Psi_n(\beta_2) - m_2 \Psi_n(\beta_3) \\ U_3 &= m_0 \Psi_n(\beta_0) - m_1 X_n(\beta_1) \\ U_4 &= m_0 \Psi_n(\beta_0) - m_1 \Psi_n(\beta_1) \end{aligned}$$

$$\begin{aligned} U_5 &= m_0 X_n(\beta_0) - m_1 X_n(\beta_1) \\ U_6 &= m_0 X_n(\beta_0) - m_1 \Psi_n(\beta_1) \\ U_7 &= m_0 X_n(\beta_1) - m_1 \Psi_n(\beta_0) \\ U_8 &= m_0 \Psi_n(\beta_1) - m_1 \Psi_n(\beta_0) \\ U_9 &= m_1 \Psi_n(\beta_3) - m_2 \Psi_n(\beta_2) \\ U_{10} &= m_1 \Psi_n(\beta_3) - m_2 X_n(\beta_2) \\ U_{11} &= m_0 X_n(\beta_1) - m_1 X_n(\beta_0) \\ U_{12} &= m_0 \Psi_n(\beta_1) - m_1 X_n(\beta_0) \end{aligned}$$

Here we set

$$\begin{aligned} \beta_0 &= m_0 \alpha_1 \\ \beta_1 &= m_1 \alpha_1 \\ \beta_2 &= m_1 \alpha_2 \\ \beta_3 &= m_2 \alpha_2 \end{aligned}$$

and $\alpha_1 = 2\pi b/\lambda$ and $\alpha_2 = 2\pi a/\lambda$.

It is straightforward to show that the solution for the homogeneous cylinder is obtained directly from (10) and (11). For this case, $\beta_1 = \beta_2 = \beta_3$ and $m_1 = m_2$, and we obtain

$$\begin{aligned} b_n^0 &= \frac{J_n(\beta_0) U_4}{H_n(\beta_0) U_6} \\ a_n^0 &= \frac{J_n(\beta_0) U_8}{H_n(\beta_0) U_{12}} \end{aligned} \quad (12)$$

and with suitable substitution for U_4 , U_6 , U_8 , and U_{12} the expression for b_n^0 and a_n^0 for homogeneous cylinders is obtained. These formula were used to provide a convenient check on the numerical solutions as $m_1 \rightarrow m_2$.

3. SCATTERING CROSS SECTIONS AND PHASE FUNCTIONS

The formula for the scattering and extinction efficiencies and the scattering phase functions is derivable directly from the b_n^0 and a_n^0 coefficients [e.g., Bohren and Huffman, 1983] for unpolarized incident radiation. Examples of the extinction efficiency obtained from these coefficients and the single-scatter albedo $\tilde{\omega}_0$, defined here as

$$\tilde{\omega}_0 = Q_{\text{scat}}/Q_{\text{ext}}$$

are plotted in Figure 4 as a function of the size parameter $\chi = kb$. Two wavelengths are chosen to illustrate the results. One corresponds to the case of weak absorption ($2.3 \mu\text{m}$) and the second to the case of strong absorption ($11 \mu\text{m}$). Figure 4 shows the scattering parameters derived for each of these wavelengths for a solid cylindrical scatterer (solid curves on all diagrams) and a hollow ice cylinder with its volume reduced to 70% of the solid particle. The 30% reduction in volume chosen for these illustrations is somewhat typical of the reduction in the crystal density expected from Figure 2.

The most striking feature evident in the comparisons of Q_{ext} is the change in the positions of the diffraction maxima and minima. These extrema result from the constructive and destructive interference of the incident wave (on some distant reference plane) and the scattered wave which has undergone some change in phase. For the hollow particle these extrema are shifted to higher values of χ as a result of the reduced change in phase of this transmitted wave. As could be anticipated, these differences are most acute for the nonabsorbing

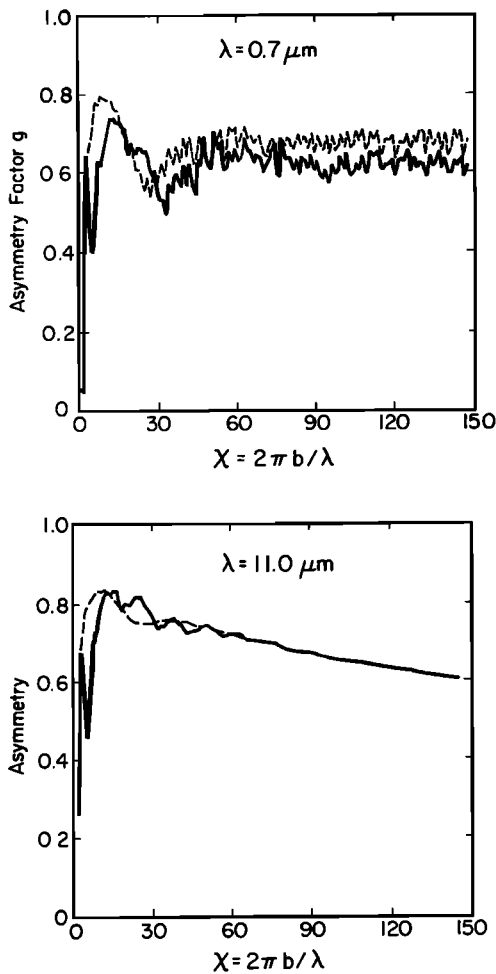


Fig. 6. The asymmetry parameter as a function of the outer shell size parameter (kb). The solid and dashed curves are as in Figure 5: (top) $\lambda = 0.7 \mu\text{m}$; (bottom) $\lambda = 11.0 \mu\text{m}$.

(not shown) and the weakly absorbing case ($\lambda = 2.3 \mu\text{m}$) but are not as apparent for strongly absorbing particles ($\lambda = 11\text{-}\mu\text{m}$ case), especially for $\chi \gtrsim 25$. The single-scatter albedo for $\lambda = 2.3 \mu\text{m}$ also reveals some differences between the solid and hollow crystal and is greater for the hollow particle. That is, the absorption by the hollow particle is less than that of the solid particle. For $11\text{-}\mu\text{m}$ radiation the effects of crystal porosity again have no real effect on the absorption, especially when $\chi \gtrsim 25$.

While results shown in Figures 4a and 4b apply only for radiation that is normally incident on the particle, it is possible to infer the expected effects for other directions of incidence. The path of an obliquely incident ray through the crystal is longer than that for a normally incident ray. The lag thus produced for oblique incidence is therefore greater and the positions of the maxima and minima in the extinction curve will change relative to normal incidence, much in the same way as shown for solid cylinders by Stephens [1984]. However, as was demonstrated by Stephen's, on averaging over orientation (and thus all sets of incident angles), size distribution, and wavelength, the maxima interference and minima features smooth out and the effect of the orientation of the incident wave, not to mention the differences between solid and hollow cylinder, are thus reduced, especially for sufficiently large values of χ (say, $\sigma \gtrsim 10$). For strongly absorbing

wavelengths the differences between solid and hollow particles and normal and oblique incidence again can be expected to be almost negligible for $\chi \gtrsim 10$ (refer to Figure 4b).

Comparisons of the scattering phase function for the solid and hollow ice cylinder normally illuminated by unpolarized radiation are shown in Figure 5 as a function of scattering angle θ for the two wavelengths $\lambda = 0.7 \mu\text{m}$ and $\lambda = 11 \mu\text{m}$. The influence of crystal porosity, through its effect on the phase of the radiation scattered by the crystal at an angle θ is apparent from the diagrams in Figure 5. Also apparent is the enhanced diffraction in the forward direction for the hollow particle. This stronger forward scatter for hollow particles results in greater values of asymmetry parameters, defined here as

$$g = \frac{1}{2} \int_{-1}^{+1} \rho(\theta) \cos \theta d\theta \quad (13)$$

and illustrated in Figure 6 as a function of α_1 , using the phase functions depicted in Figure 5.

4. DISCUSSION AND CONCLUSIONS

The major issue addressed in this paper is how the effects of ice crystal porosity might influence the scattering characteristics of an ice particle in clouds. The essential conclusion drawn from the results described previously is that the scattering properties of a hollow cylinder, and perhaps more complex hollow particles, are not greatly different from the properties deduced from an equivalent homogeneous particle. While the difference in the positions of the interference maxima and minima of extinction efficiency is significant for an individual particle, these differences are removed on averaging over particle size distribution and orientation.

Even though the effect of porosity on single-scatter properties is small, one could anticipate that its influence on the relationships between cloud albedo, shortwave absorption, and emissivity on the IWP to be substantial. The results of this study suggest that the influence is largely a result of the effect of crystal porosity on the specification of IWP and not on the specification of the single-scattering properties of the crystal. The tendency for the observed ε -IWP relationships, such as they are, to predict significantly smaller values of ε for any given IWP than theory would allow may well arise not from errors in the measured radiative fluxes from which ε is deduced, nor from some absorption incorrectly over accounted for in the theory, but simply from inaccurate estimates of ice water paths. In this context it is relevant to note that neither of the observational studies mentioned in relation to Figure 1 considered the relationships between crystal size and density (as shown in Figure 2, for example) in estimating IWP.

Acknowledgments. This work was supported by the Atmospheric Sciences Section of the National Science Foundation under contract ATM-8519160 and the computer calculations were carried out using the computer facilities at the National Center for Atmospheric Research, which is supported by the National Science Foundation. I also gratefully acknowledge the efforts of Susan Lini, who prepared the manuscript.

REFERENCES

- Bohren, C. F., and D. R. Huffman, *Absorption and Scattering of Light by Small Particles*, p. 550, John Wiley, New York, 1983.
- Chylek, P., and V. Ramaswamy, Simple approximation for infrared emissivity of water clouds, *J. Atmos. Sci.*, 39, 171-177, 1982.
- Griffith, K., S. K. Cox, and R. G. Kollenberg, Infrared properties of

- tropical cirrus clouds inferred from aircraft measurements, *J. Atmos. Sci.*, *37*, 1077–1087, 1980.
- Heymsfield, A. J., Ice crystal terminal velocities, *J. Atmos. Sci.*, *29*, 1348–1357, 1972.
- Heymsfield, A. J., Precipitation development in stratiform ice clouds: A microphysical and dynamical study, *J. Atmos. Sci.*, *34*, 367–381, 1977.
- Heymsfield, A. J., and R. J. Knollenberg, Properties of cirrus generating cells, *J. Atmos. Sci.*, *34*, 1358–1366, 1972.
- Heymsfield, A. J., and C. M. R. Platt, Parameterization of the particle size spectrum of ice clouds in terms of the ambient temperature and ice water content, *J. Atmos. Sci.*, *41*, 846–855, 1984.
- Kerker, M., and E. Matijevic, Scattering of electromagnetic waves from concentric infinite cylinder, *J. Opt. Soc. Am.*, *51*, 506–508, 1961.
- Liou, K-N., and G. D. Wittman, Parameterization of radiative properties of clouds, *J. Atmos. Sci.*, *36*, 1261–1273, 1979.
- Paltridge, G. W., and C. M. R. Platt, Aircraft measurements of solar and infrared radiation and their microphysics of cirrus cloud, *Q. J. R. Meteorol. Soc.*, *102*, 512–522, 1981.
- Platt, C. M. R., N. L. Abshire, and G. T. McNice, Some microphysical properties of an ice cloud from lidar observations of horizontally oriented crystals, *J. Appl. Meteorol.*, *8*, 1220–1224, 1978.
- Pruppacher, H., and J. Klett, *Microphysics of Clouds and Precipitation* 714 pp., D. Reidel, Hingham, Mass., 1980.
- Ramanathan, V., E. J. Pitcher, R. C. Malone, and M. L. Blackman, The response of a spectral general circulation model to refinements in radiative processes, *J. Atmos. Sci.*, *40*, 605–630, 1983.
- Samaddor, S. N., Scattering of plane electromagnetic waves by radially inhomogeneous infinite cylinders, *Il Nuovo cimeto*, *46*, 33–50, 1970.
- Starr, D. O. and S. K. Cox, Cirrus clouds, I and II, *J. Atmos. Sci.* *42*, 2663–2694, 1985.
- Stephens, G. L., Radiative properties of extended water clouds, I and II, *J. Atmos. Sci.*, *35*, 2111–2132, 1978.
- Stephens, G. L., The scattering of plane waves by soft obstacles, Anomalous diffraction theory for circular cylinders. *J. Appl. Opt.*, *23*, 954–959, 1984.

G. L. Stephens, Department of Atmospheric Sciences, Colorado State University, Fort Collins, CO 80526.

(Received February 4, 1986;
revised November 7, 1986;
accepted November 13, 1986.)